Supporting Information

Ultrahigh Stable Laminar Graphene Membranes for Effective Ionic and Molecular Nanofiltration with Machine Learning-Assisted Study

Poonsawat Paechotrattanakul [1], Kulpavee Jitapunkul [2], Pawin Iamprasertkun [2], Pannaree Srinoi [1], Weekit Sirisaksoontorn [1,*], Wisit Hirunpinyopas [1,*]

[1] Department of Chemistry and Centre of Excellence for Innovation in Chemistry, Faculty of Science, Kasetsart University, Chatuchak, Bangkok, 10900 Thailand

[2] School of Bio-Chemical Engineering and Technology, Sirindhorn International Institute of Technology, Thammasat University, Pathum Thani, Thailand

Keywords: membrane, graphene, ionic sieving, water purification, machine learning

***Corresponding author;**

e-mail: fsciwks@ku.ac.th (W. Sirisaksoontorn), wisit.hi@ku.ac.th (W. Hirunpinyopas)

Contents:

1. The graphene thickness from TEM analysis

The TEM image of the graphene dispersion is shown in Figure S1. The number of graphene layers are mostly 8–10 layers with a d-spacing of 0.34 nm corresponding to the PXRD analysis.

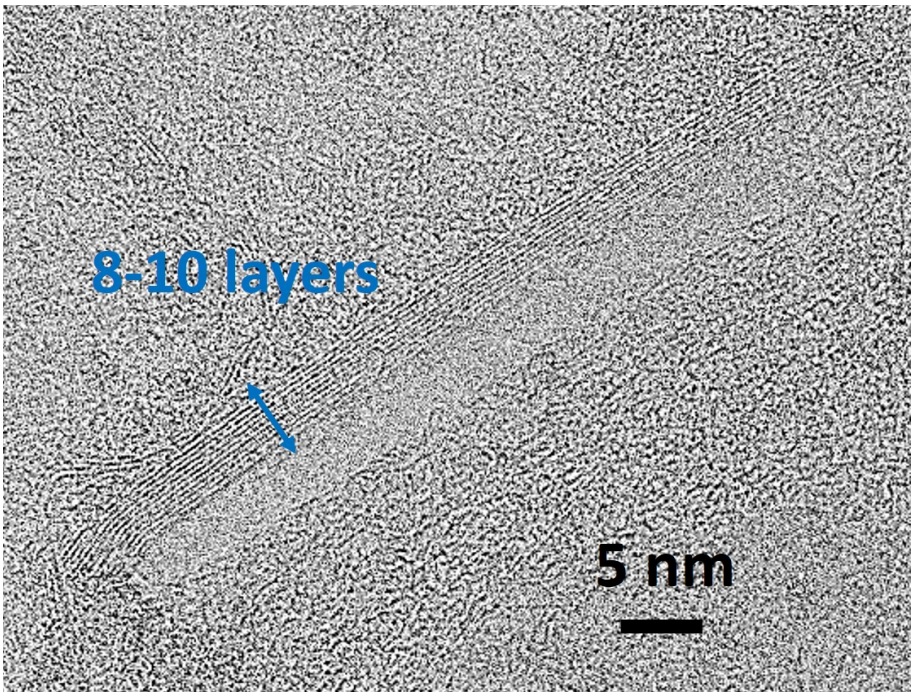

Figure S1. TEM image showing the number of graphene layer (ca. 8-10 layers).

2. The stability of the graphene membranes

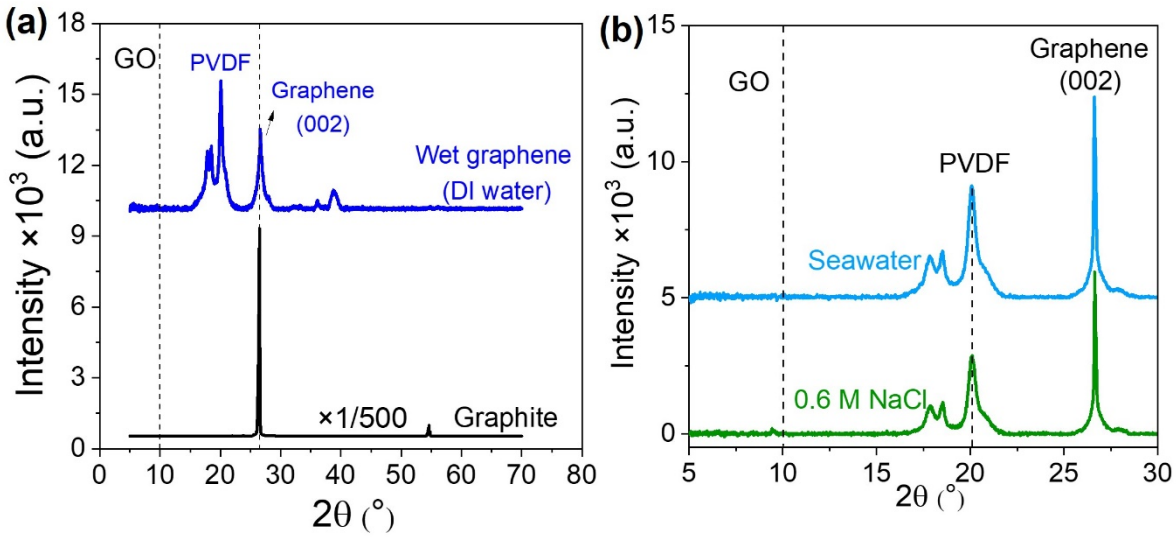

Figure S2. (a) The full PXRD pattern of starting material (bulk graphite) showing high crystallinity at (002) plane, as well as the wet graphene membrane after immersed in DI water showing a broader (002) peak with the absence of characteristic GO diffraction at 2θ of ~10°. (b) Comparing PXRD patterns of the wet membranes after immersed in 0.6 M NaCl and seawater for over 8 days.

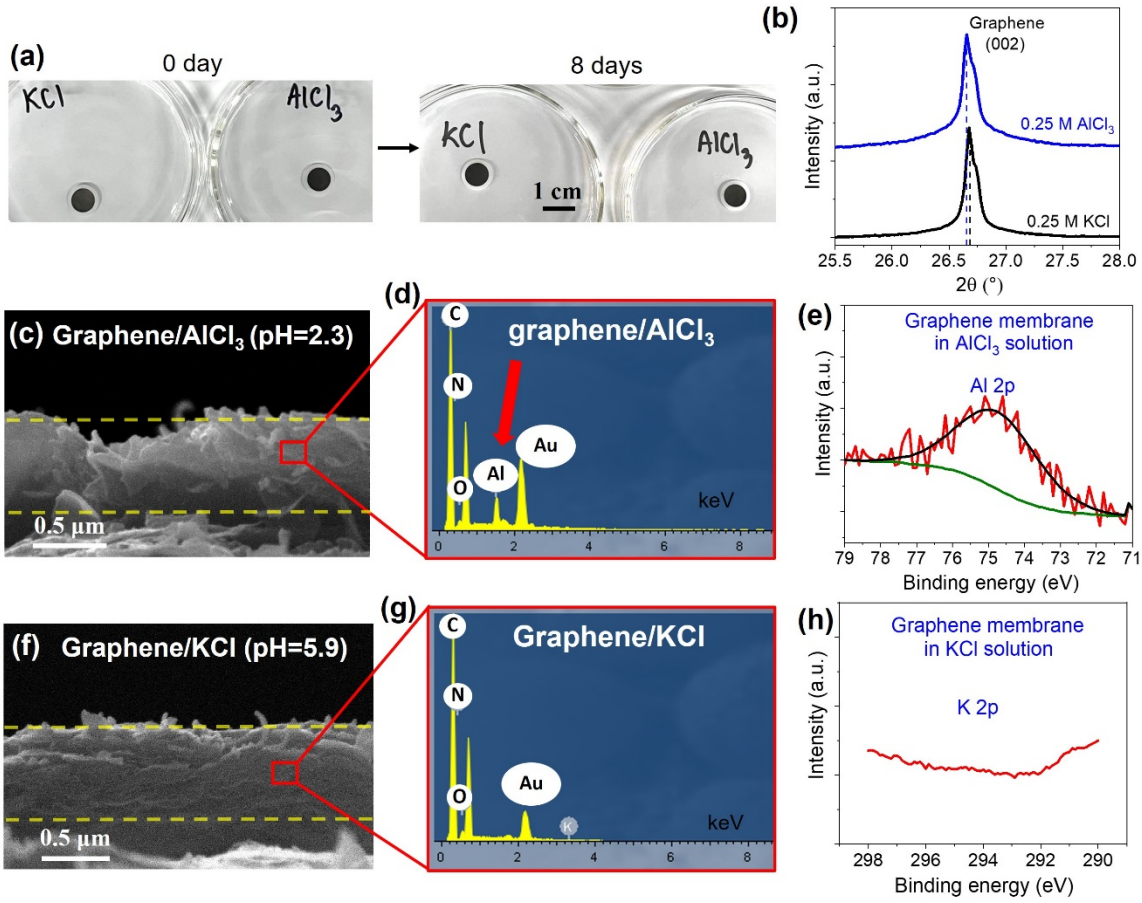

Figure S3. The membrane stability in aqueous salt solutions. (a) Photographs of the graphene membranes before and after immersed in KCl and $AlCl_3$ solutions for 8 days, in which the membranes remain intact. (b) PXRD patterns of the membranes after immersed in KCl and $AlCl_3$ solutions. (c) The corresponding cross-sectional SEM image after immersed in $AlCl_3$ solution with (d) its EDS spectrum showing C, N, O, and Al elements inside lamellar structure, and (e) XPS spectrum of Al 2p. (f) The corresponding cross-sectional SEM image after immersed in KCl solution with (g) its EDS spectrum showing C, N, and O elements, and (h) XPS spectrum of K 2p.

To further investigate the stability of the graphene membrane, the membranes were tested in 0.25 M KCl and $AlCl_3$ solutions for over 8 days. After that, the membranes were cleaned by soaking in DI water for at least 30 min to remove any residual salt solutions. The results show that the membranes remain intact (see Figure S3a). In Figure S3b, the PXRD pattern of the membrane after immersed in $AlCl_3$ solution exhibits a tiny shift of the (002) peak toward lower 2θ, which indicates the slight increase in the height of capillary channels. This is due to the effect of intercalation between hydrated Al^{3+} cation (4.75 Å in radii) and the lamellar graphene membranes, as confirmed by elemental analysis using EDS and XPS

(Figures S3c-e). The presence of Al^{3+} in the lamellar structure can be explained by a a cation-π interaction between the hydrated Al^{3+} and the surface of graphene nanosheets, as previously reported in GO membranes using cation control of interlayer spacing.[1-3] However, the K^+ inside the membrane cannot be detected by both techniques after immersed in KCl solution (Figures S3f-h). This is due to a nature of a very small hydrated K^+ cation (3.31 Å in radii) and the high diffusion coefficient of K^+,[4, 5] which can easily transport out from the capillary channels inside the membrane during the cleaning process.[6, 7]

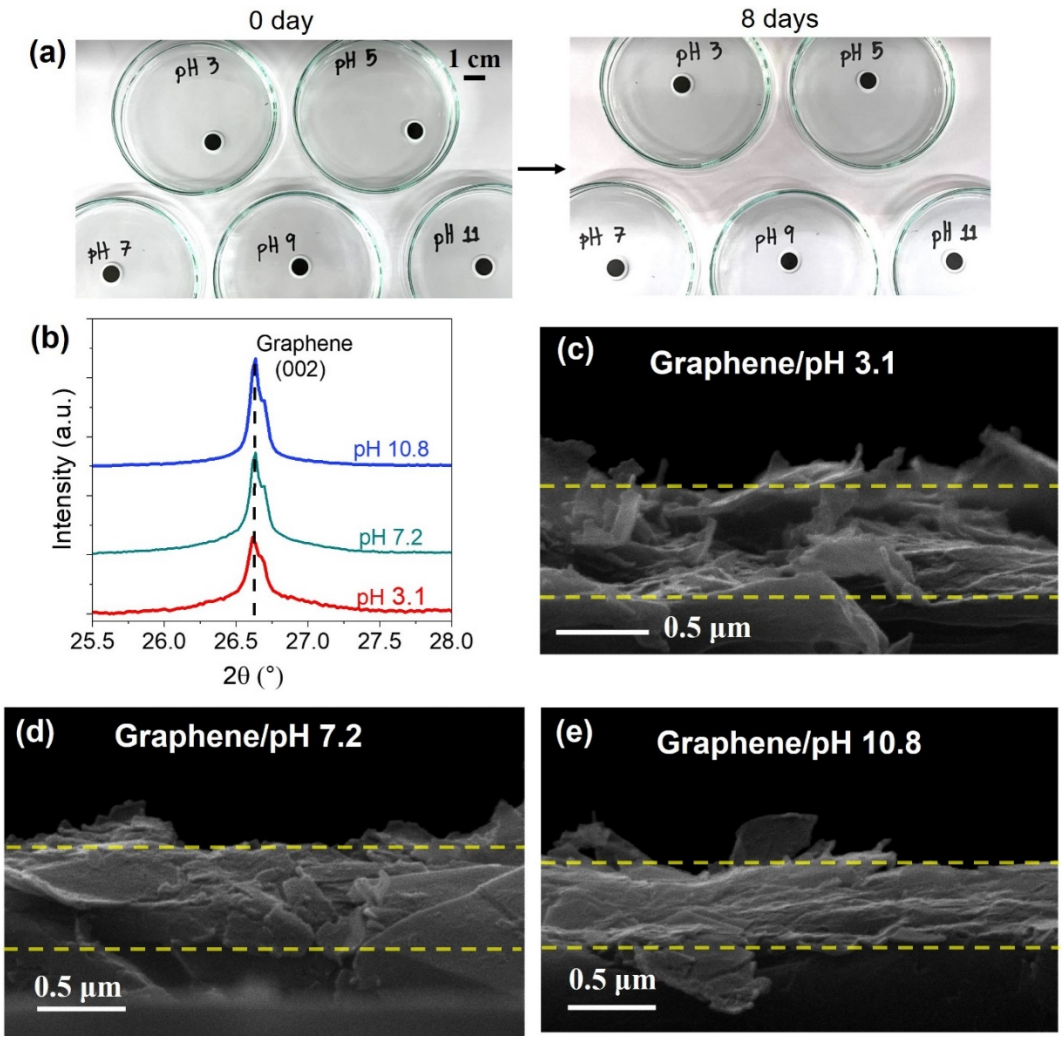

Figure S4. The membrane stability in various pH conditions. (a) Photographs of the graphene membranes before and after immersed in pH 3.1-10.8 for 8 days, in which the membranes remain intact. (b) PXRD patterns of the membranes after immersed in different pH. (c-e) Corresponding cross-sectional SEM images after immersed in pH 3.1, 7.2, and 10.8, respectively.

Moreover, the stability of the graphene membrane was also tested in various pH conditions. The membranes remain intact after immersed in pH ranging from 3.1 to 10.8 for over 8 days (Figure S4a). It was found that neither the (002) PXRD patterns (Figure S4b) nor cross-sectional SEM images (Figures S4c-e) exhibit any significant difference in the lamellar graphene structure, indicating the excellent membrane stability.

3. Thickness calibration of graphene membranes

Figure S5 shows the thickness calibration of each graphene-based membrane. Three different mass loadings were used to measure the thicknesses using cross-sectional scanning electron microscopy (SEM). It is clearly seen that the thickness of graphene laminate increased with increasing graphene mass loading, as shown in Figures S5a-c. Moreover, the mass loading and density of the membranes in each thickness were also calculated as shown in Table S1. It reveals that the average membrane density for three different thicknesses was *ca*. 1.54 g cm^{-3}, while the density of bulk graphite was 2.09-2.23 g cm^{-3}. This indicated the large amount of capillary channels within the graphene membranes, which were estimated to be 26-31%.

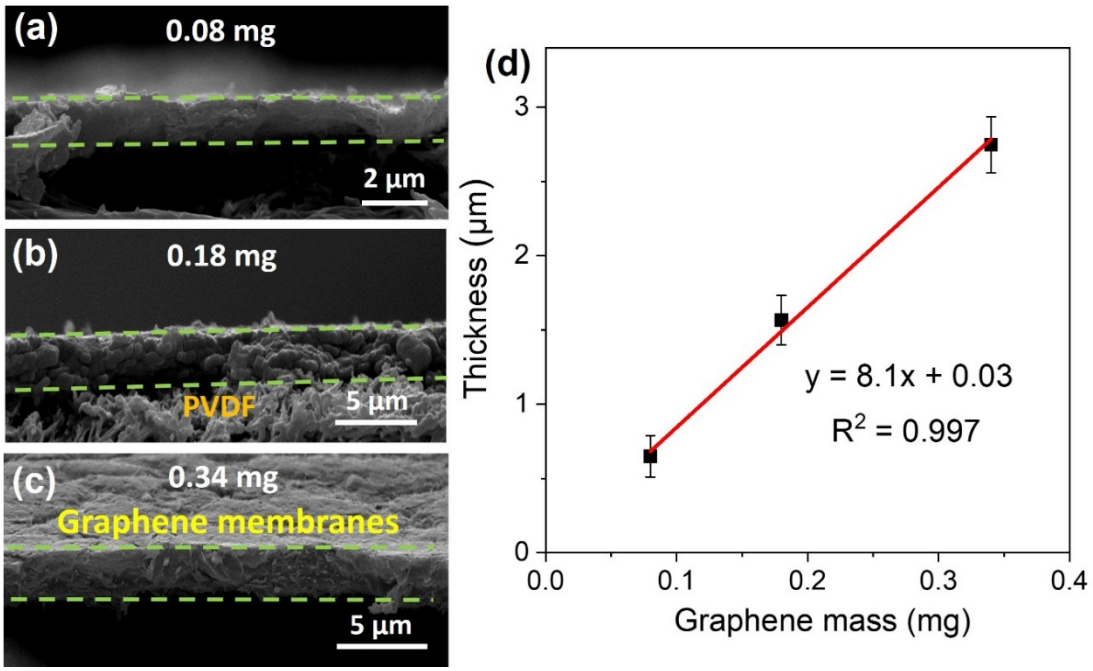

Figure S5. The graphene-based membrane thickness calibration. (a-c) SEM cross-section of graphene based membranes at three different mass loading. (d) The correlation between the mass of graphene loading and the graphene thickness. The red line represents the linear relationship between graphene mass and the corresponding thickness with the linear equation. Error bars are the standard deviation of graphene thickness obtained by the thickness measurement throughout the membrane.

Table S1. The density of graphene membranes in each thickness.

Mass of graphene membrane (mg)	**Thickness (μm)**	**Density (g cm^{-3})**
0.08	0.65 ± 0.14	1.57
0.18	1.56 ± 0.17	1.47
0.34	2.75 ± 0.19	1.57
		Aver = 1.54

Note the density of bulk graphite is 2.09 - 2.23 g/cm^{-3}.

4. Machine learning study for ion permeability

Table S2: Number of epochs with minimum validation error from all ANN architectures with 10 trials of training.

Nodes / Trials	1	2	3	4	5
1	6	44	1000	51	35
2	9	144	51	31	179
3	8	12	102	119	88
4	5	129	160	84	10
5	8	40	74	92	72
6	7	30	21	291	417
7	9	44	97	63	43
8	5	8	1000	71	114
9	7	42	69	201	127
10	11	38	16	109	239

Table S3: Coefficient of determination (R^2) from all ANN architectures with 10 trials of training.

Nodes / Trials	1	2	3	4	5
1	0.9429	0.9857	0.9916	0.9953	0.9952
2	0.9435	0.9754	0.9884	0.9794	0.9975
3	0.9432	0.9451	0.9882	0.9864	0.9881
4	0.9291	0.9754	0.9853	0.9877	0.9867
5	0.9401	0.9858	0.9903	0.9962	0.9932
6	0.9436	0.9647	0.9938	0.9976	0.9976
7	0.9441	0.9857	0.9882	0.9861	0.9919
8	0.9380	0.9315	0.9926	0.9902	0.9936
9	0.9437	0.9857	0.9904	0.9917	0.9978
10	0.9432	0.9857	0.9939	0.9899	0.9987

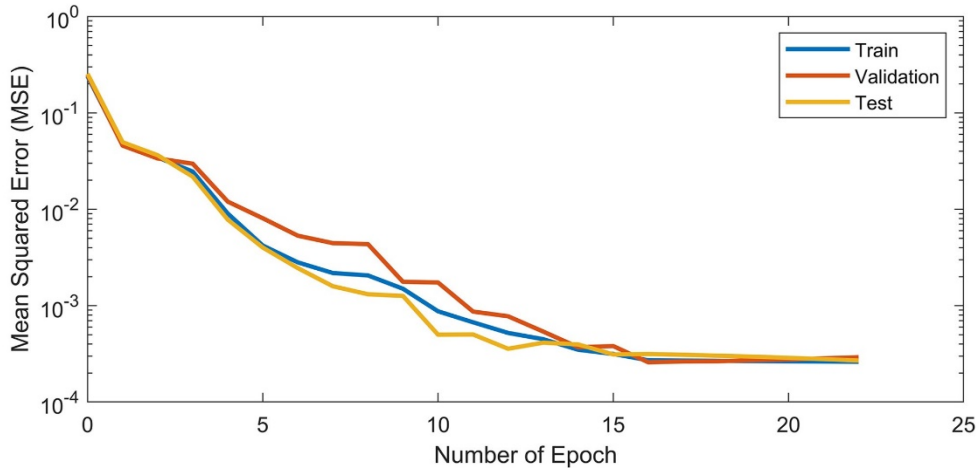

Figure S6. Learning curves of shallow artificial neural network (ANN) with 3 hidden nodes for studying ionic sieving through the graphene membranes. The blue, red, and yellow solid lines represent the trained, validation, and tested samples, respectively.

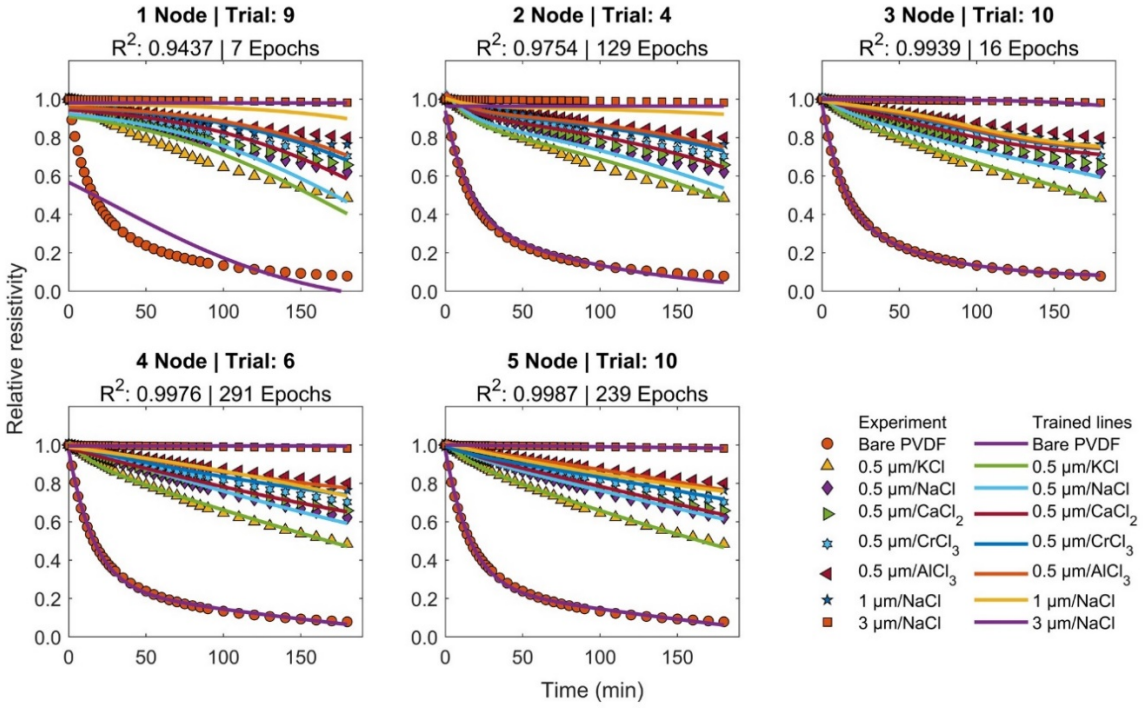

Figure S7. Relative resistivity plots versus time at different graphene thickness in various salt solutions from best training of each network architecture. The experimental data are presented as scatter plots with different markers. The trained data is plotted with solid lines. The coefficient of determination (R^2), number of epochs, and trial number of the best model in each network architecture (1 to 5 hidden nodes) were indicated above each subplot.

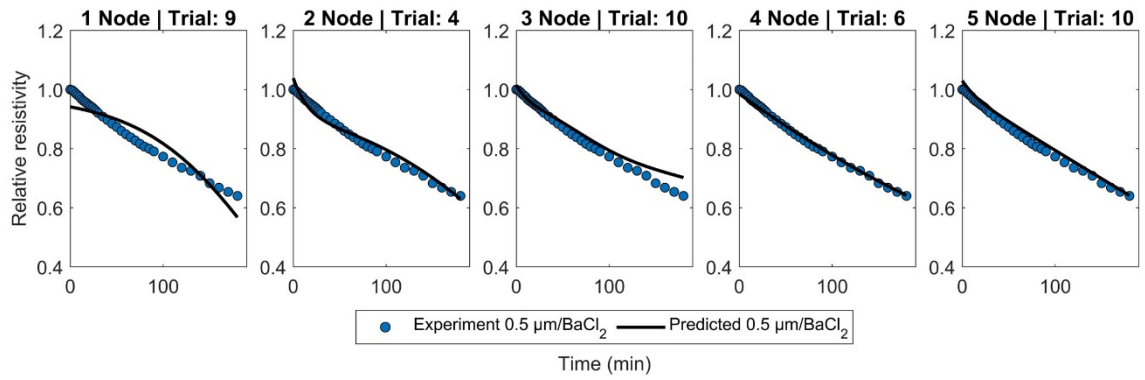

Figure S8. Relative resistivity plot versus time of 0.5 μm-thick graphene membrane in $BaCl_2$ solution. The experimental data are presented as a scatter plot while the predicted data from a selected model of each network architecture is plotted as the black solid line.

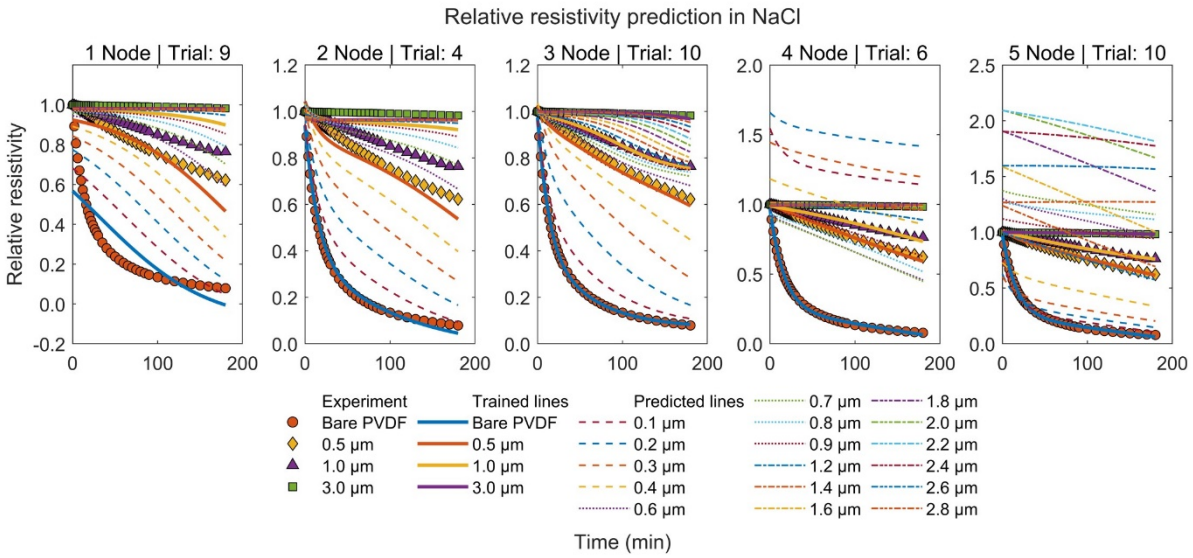

Figure S9. Prediction of NaCl ion permeability with graphene membrane thickness ranging from 0.1 to 3 μm. Each subplot presents the predicted data in comparison with trained data and experimental data of selected trials from each network architecture.

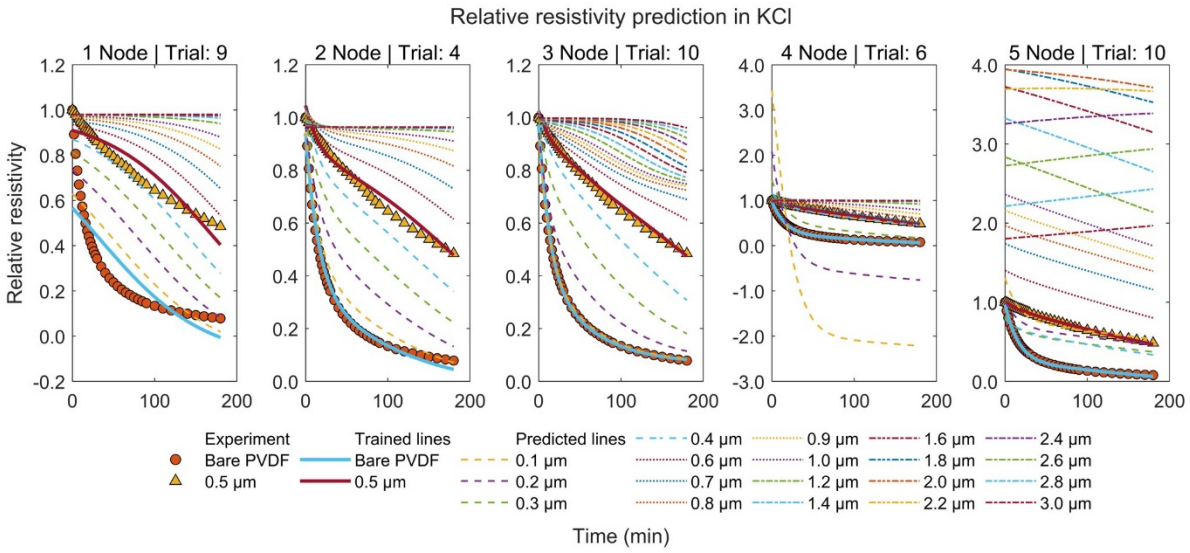

Figure S10. Prediction of KCl ion permeability with graphene membrane thickness ranging from 0.1 to 3 μm. Each subplot presents the predicted data in comparison with trained data and experimental data of selected trials from each network architecture.

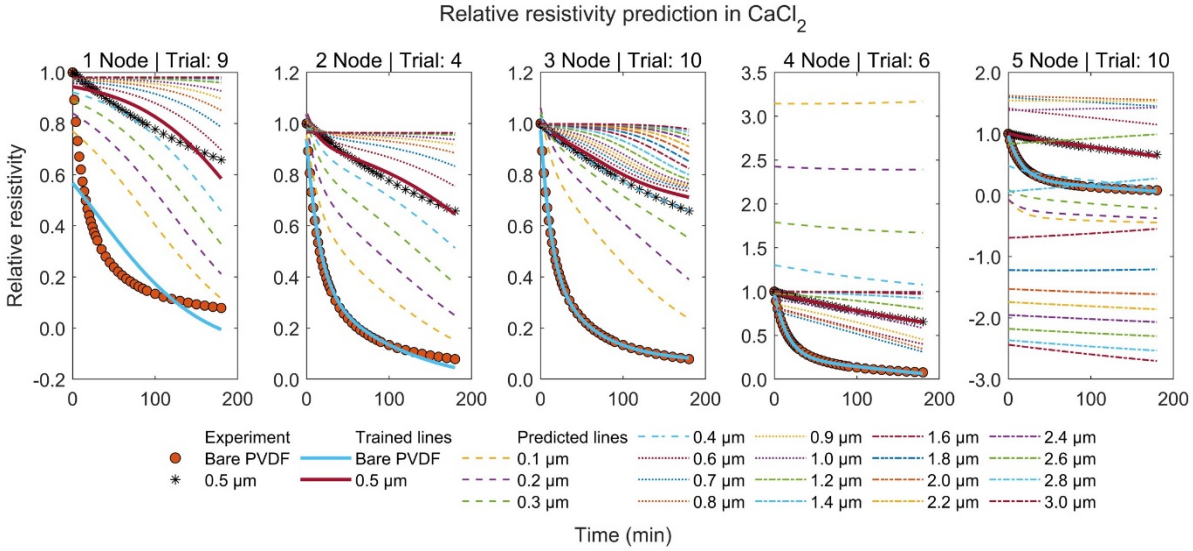

Figure S11. Prediction of $CaCl_2$ ion permeability with graphene membrane thickness ranging from 0.1 to 3 μm. Each subplot presents the predicted data in comparison with trained data and experimental data of selected trials from each network architecture.

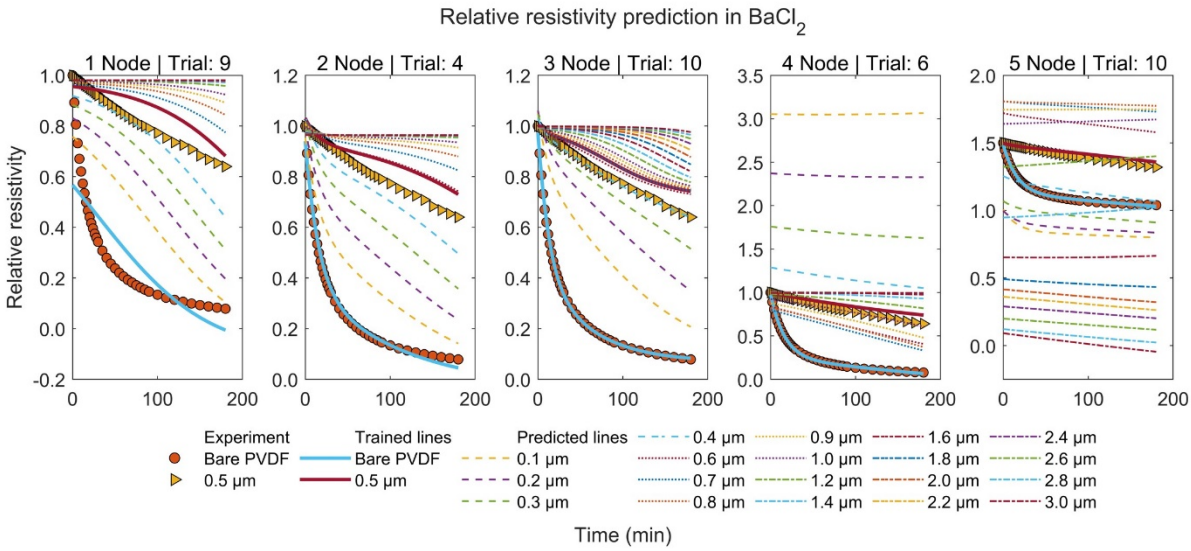

Figure S12. Prediction of $BaCl_2$ ion permeability with graphene membrane thickness ranging from 0.1 to 3 μm. Each subplot presents the predicted data in comparison with trained data and experimental data of selected trials from each network architecture.

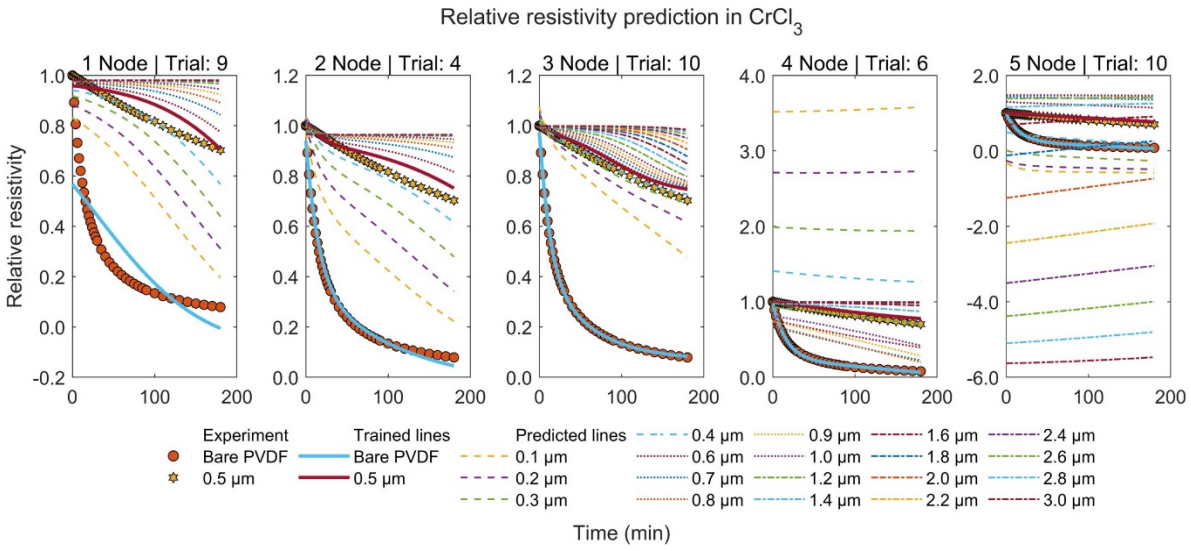

Figure S13. Prediction of $CrCl_3$ ion permeability with graphene membrane thickness ranging from 0.1 to 3 μm. Each subplot presents the predicted data in comparison with trained data and experimental data of selected trials from each network architecture.

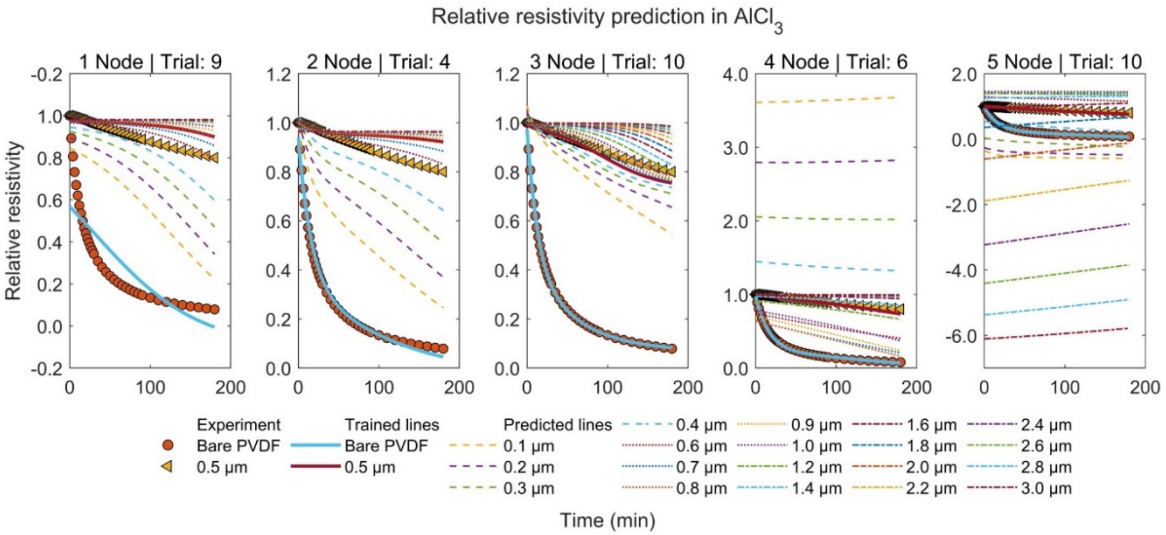

Figure S14. Prediction of $AlCl_3$ ion permeability with graphene membrane thickness ranging from 0.1 to 3 μm. Each subplot presents the predicted data in comparison with trained data and experimental data of selected trials from each network architecture.

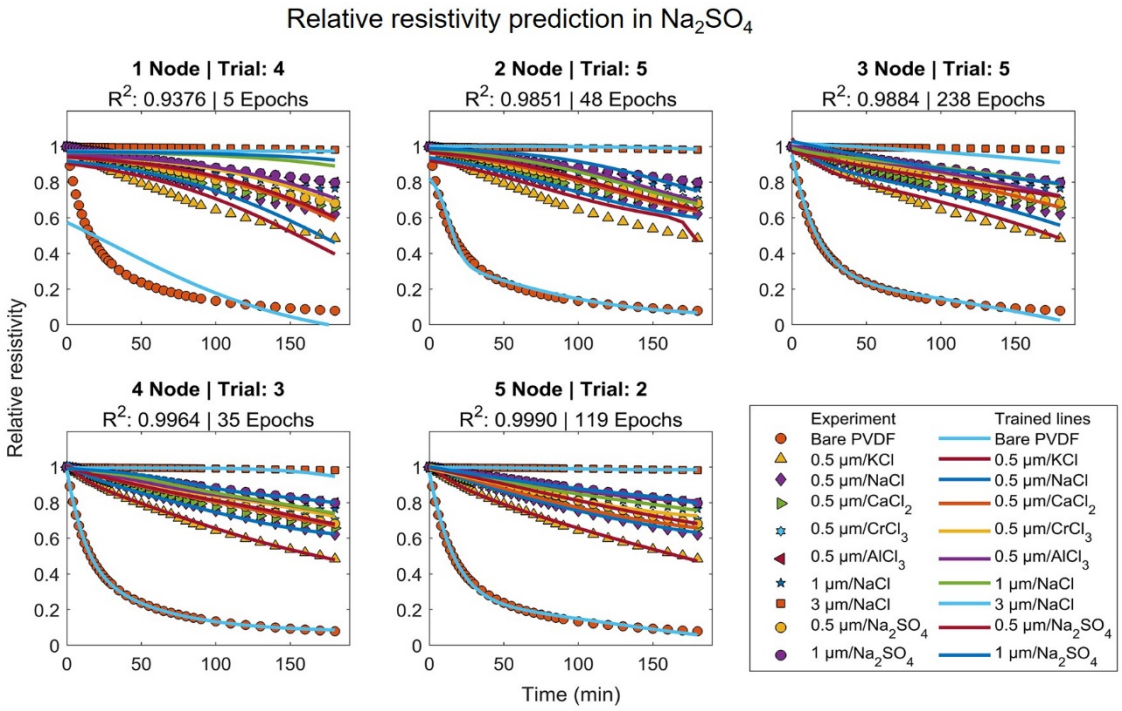

Figure S15. Relative resistivity plots versus time at different graphene thicknesses in various chloride solutions and Na_2SO_4 salt from the best training of each network architecture. The experimental data are presented as scatter plots with different markers. The trained data were plotted with solid lines. The coefficient of determination (R_2), number of epochs, and trial

number of the best model in each network architecture (1 to 5 hidden nodes) were indicated above each subplot.

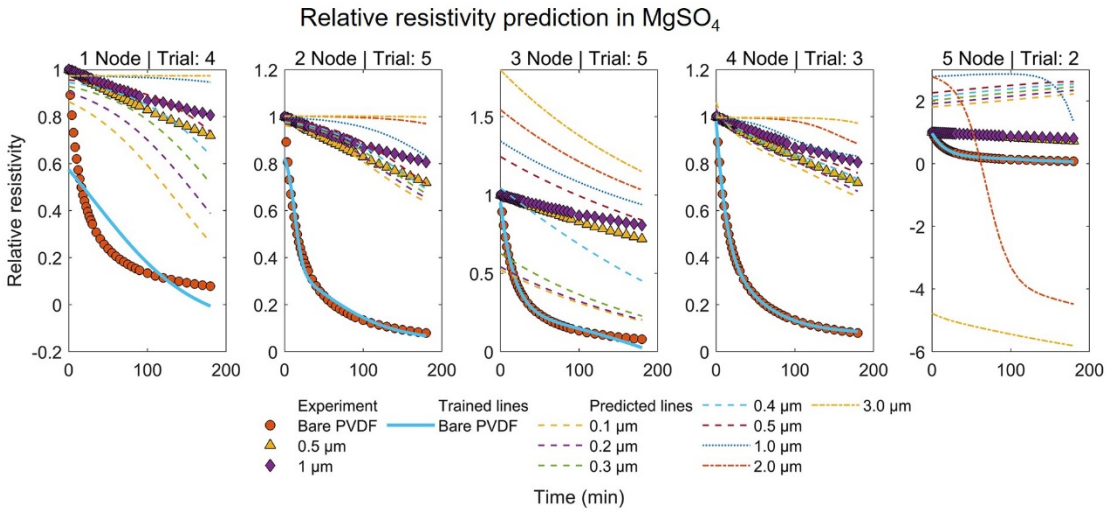

Figure S16. Prediction of $MgSO_4$ ion permeability with the thickness of graphene membranes ranging from 0.1 to 3 μm. Each subplot presents the predicted data in comparison with experimental data of selected trials from each network architecture.

5. Measurement of dye rejection

The measurement of dye rejection and water permeation rate was also performed using the forward osmosis pressure technique.[8, 9] The graphene membrane at 0.5 μm-thick was then sealed between two containers with equal volumes (10 ml) of 1 M sucrose aqueous solution on one side of the membrane (permeate side) and 30 ppm dyes (i.e. acid orange 7 (AO7), methyl orange (MO), methylene blue (MB), and methyl red (MR)) on the other side (feed side). The experiment was performed for 20 h to measure an increase in solution volume and dye molecules in the sucrose side (the draw side). The dye rejection was determined by measuring absorbance using UV-vis spectroscopy. The dye rejection (R_{dye}%) was calculated using $1 - C_p/C_f$ where C_p and C_f are the concentration of dye in the permeate and feed sides, respectively.[7, 9] The rejection and the water flow rates of four dyes were determined from at least two different sets of membranes, as shown in Table S4. Comparing between AO7 and MO possessing negatively charged molecules with the comparable size,[10, 11] the membrane can reject AO7 to the greater extent than MO due to the effect of size exclusion (see Figures S17a-b). This can also be explained for the rejection of MB and MR.[11,

[12] Comparing between AO7 and MB as negatively and positively charged molecules, respectively, the rejection performance for AO7 is slightly higher than that for MB, resulting from the electrostatic repulsion between negatively charged graphene and AO7 molecules (Figure S17). The average water flow rates for four dyes are ca. 5×10^{-3} L m^{-2} h^{-1} bar^{-1}.

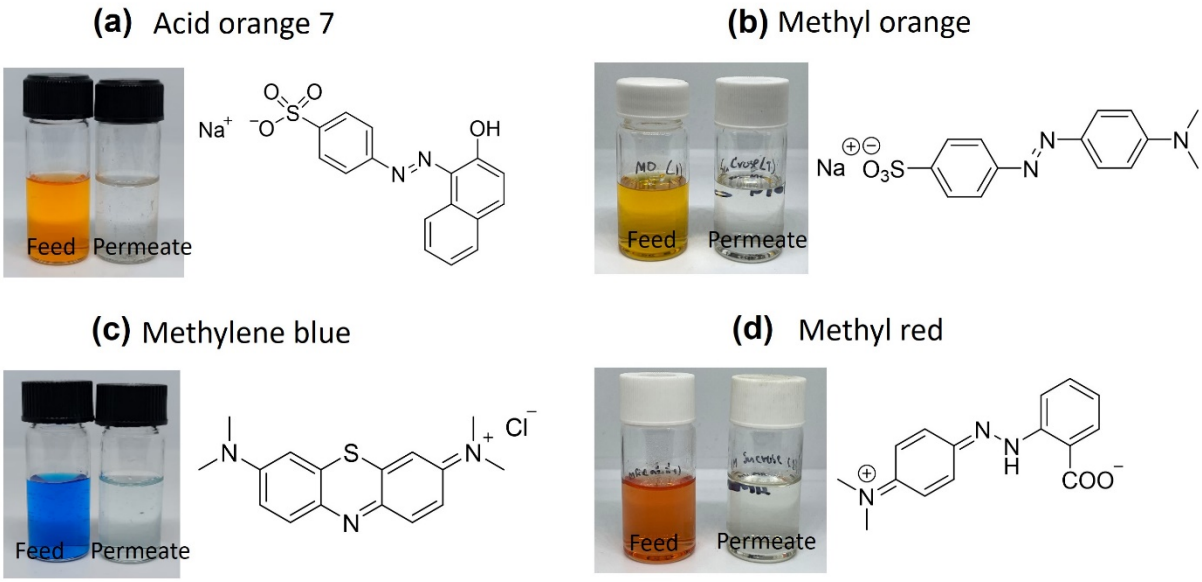

Figure S17. Dye rejection performance by forward osmotic pressure. Photographs of (a) acid orange 7, (b) methyl orange, (c) methylene blue, and (d) methyl red before and after filtration by 0.5 μm-thick graphene membranes with their corresponding charged dye molecules.

Table S4. Ionic rejection and water permeation rate of acid orange 7, methyl orange, methylene blue, and methyl red.

Molecule	**Dimensional size**	**Dye rejection (%)**	**Water permeation rate (10^{-3} L m^{-2} h^{-1} bar^{-1})**
Acid orange 7	5.4 × 10.0 × 15.7 Å (ref[10])	99.1 ± 0.4	4.8 ± 0.9
Methyl orange	12.0 × 10.0 Å (ref[11])	98.0 ± 0.3	5.0 ± 0.7
Methylene blue	3.3 × 7.6 × 17.0 Å (ref[12])	97.9 ± 0.3	4.2 ± 0.9
Methyl red	11.0 × 8.0 Å (ref[11])	95.1 ± 1.3	5.4 ± 0.3

6. Conductance of graphene laminates

The conductance of the solely graphene laminates were experimentally calculated by the conductance of each ion after subtracting the conductance measured for the same electrolyte in a bare PVDF membrane as follows:

$$G = \frac{\Delta I}{\Delta V} \quad \text{(S1)}$$

On the basis of electrical conductance, it can be expressed as a reciprocal value to resistance. Then, the total conductance of a series circuit between a graphene membrane and a bare PVDF ($G_{graphene|PVDF}$) can be calculated from the individual conductance contributing from a solely graphene ($G_{graphene}$) and a bare PVDF (G_{PVDF}) as shown in the following equation:

$$\frac{1}{G_{graphene|PVDF}} = \frac{1}{G_{graphene}} + \frac{1}{G_{PVDF}} \quad \text{(S2)}$$

By using this equation, the conductance contribution from the graphene membranes can be estimated as:

$$G_{graphene} = \frac{G_{PVDF}G_{graphene|PVDF}}{G_{PVDF} - G_{graphene|PVDF}} \quad \text{(S3)}$$

7. Ion permeation under pH dependence

To further investigate the role of the adsorption of hydronium (H_3O^+) and hydroxide ions (OH^-) on the graphene membrane, Figure S18a shows the *I-V* responses of the membranes using a constant KCl concentration in aqueous solutions for both sides (100 mM) at a wide range of pH values (pH 3.2 to 10.4). The corresponding ionic conductance as a function of pH of the 0.5 μm-thick graphene membrane was shown in Figure S18b. The KCl conductance of the graphene membrane kept constant in acidic media as well as low basic media (pH 3.2-8.8), which corresponds no adsorption of H^+ and OH^- on the graphene channel wall. This is due to the smooth and clean surface of as-prepared pristine graphene, giving rise

to no change in the charge density inside the nanochannels, unlike the case of GO membrane.[13] However, the conductance slightly increased at a strong basic solution (pH 10.4) which indicated an increase in the OH^- adsorption on the graphene surface. This exhibited the increase in the negative charge density inside the membrane. It is in agreement with previously reported work of pristine MoS_2 membranes without any chemical functionalization.[14]

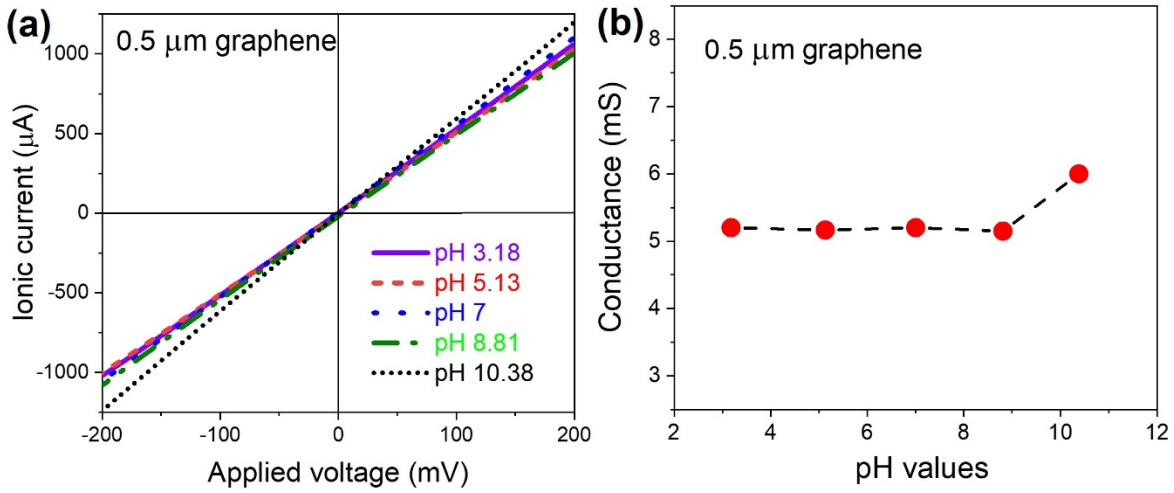

Figure S18. pH dependent properties. (a) *I*–*V* characteristics of the 0.5 µm-thick graphene membrane at a constant KCl concentration of 100 mM at different pH, from 3.18 to 10.38. (b) Corresponding conductance of the graphene membrane at various pH.

8. Supporting references

1. L. Chen, G. Shi, J. Shen, B. Peng, B. Zhang, Y. Wang, F. Bian, J. Wang, D. Li, Z. Qian, G. Xu, G. Liu, J. Zeng, L. Zhang, Y. Yang, G. Zhou, M. Wu, W. Jin, J. Li and H. Fang, *Nature*, 2017, **550**, 380–383.
2. L. Mu, Y. Yang, J. Liu, W. Du, J. Chen, G. Shi and H. Fang, *Phys. Chem. Chem. Phys.*, 2021, **23**, 14662-14670.
3. C.-N. Yeh, K. Raidongia, J. Shao, Q.-H. Yang and J. Huang, *Nat. Chem.*, 2015, **7**, 166–170.
4. J. E. R. Nightingale, *J. Phys. Chem.*, 1959, **63**, 1381-1387.
5. P. Atkins, J. d. Paula and J. Keeler, *Physical Chemistry*, Oxford University Press, Oxford, UK, 11 edn., 2018.
6. A. Esfandiar, B. Radha, F. C. Wang, Q. Yang, S. Hu, S. Garaj, R. R. Nair, A. K. Geim and K. Gopinadhan, *Science*, 2017, **358**, 511–513.
7. W. Hirunpinyopas, P. Iamprasertkun, M. A. Bissett and R. A. W. Dryfe, *Carbon*, 2020, **156**, 119-129.
8. R. K. Joshi, P. Carbone, F. C. Wang, V. G. Kravets, Y. Su, I. V. Grigorieva, H. A. Wu, A. K. Geim and R. R. Nair, *Science*, 2014, **343**, 752–754.
9. W. Hirunpinyopas, E. Prestat, S. D. Worrall, S. J. Haigh, R. A. W. Dryfe and M. A. Bissett, *ACS Nano*, 2017, **11**, 11082–11090.
10. S. Yoon, J. J. Calvo and M. C. So, *Crystals*, 2019, **9**, 17.
11. H. Ang and L. Hong, *J. Mater. Chem. A*, 2017, **5**, 20598-20602.
12. M. Arias, E. López, A. Nuñez, D. Rubinos, B. Soto, M. T. Barral and F. Díaz-Fierros, in *Effect of Mineral-Organic-Microorganism Interactions on Soil and Freshwater Environments*, eds. J. Berthelin, P. M. Huang, J. M. Bollag and F. Andreux, Springer US, Boston, MA, 1999, pp. 361-365.
13. S. Hong, C. Constans, M. V. Surmani Martins, Y. C. Seow, J. A. Guevara Carrió and S. Garaj, *Nano Letters*, 2017, **17**, 728-732.
14. W. Hirunpinyopas, E. Prestat, P. Iamprasertkun, M. A. Bissett and R. A. W. Dryfe, *2D Mater.*, 2020, **7**, 015030.